FULL PAPER

Christmas-Tree-Shaped Palladium Nanostructures Decorated on Glassy Carbon Electrode for Ascorbic Acid Oxidation in Alkaline Condition

Md. Mahmudul Hasan, Yuki Nagao*

Md. M. Hasan, Dr. Y. Nagao
School of Materials Science,
Japan Advanced Institute of Science and Technology,
1-1 Asahidai, Nomi, Ishikawa 923-1292, Japan
E-mail: ynagao@jaist.ac.jp

Supporting information for this article is given via a link at the end of the document.

Abstract: Christmas-tree-shaped Pd nanostructures were synthesized using a simple one-step electrodeposition method with no additives on a glassy carbon electrode (GCE) surface. Growth of the hierarchical nanostructures was optimized through the applied potential, deposition time, and precursor concentration. Comprehensive characterization techniques such as scanning electron microscopy (SEM), energy-dispersive X-ray spectroscopy (EDX), X-ray photoelectron spectroscopy (XPS), X-ray powder diffraction (XRD), and cyclic voltammetry (CV) were used to characterize structural features of the Christmas-tree-shaped Pd nanostructures. Our Christmas-tree-shaped Pd nanostructures showed excellent catalytic activity for ascorbic acid (AA) electro-oxidation in the alkaline condition. The modified electrode exhibited current density of 4.5 mA cm^{-2}: much higher than that of unmodified GCE (0.6 mA cm^{-2}). This simple electrodeposition technique with well-defined hierarchical Pd nanostructures is expected to offer new perspectives using Pd-based nanostructured surfaces in different research areas.

Introduction

Nanostructured metal surfaces exhibit unique physical and chemical properties, eliciting intensive research interest for their application to heterogeneous catalysis, biosensors, and electrocatalysis.[1–3] The fabrication process can control the shapes and sizes of metal nanostructures, which provide unique physical and chemical properties. Therefore, well-defined nanostructure fabrication has garnered much attention recently.[4–8] Although different solution-based metal nanoparticle syntheses and their assemblies have been developed successfully and used in diverse applications, the fabrication process requires multiple steps and/or linker molecules.[9] These linker molecules and capping agents for the preparation of nanostructure could potentially affect the surface morphology and electroanalytical activities.[10]

Electrochemical deposition is a process that offers an alternative pathway for the fabrication of clean metal nanostructure surfaces.[11] To form different metal nanostructures, electrochemical deposition techniques had been used on different substrates, particularly on a glassy carbon electrode (GCE) surface.[12,13] The GCE is widely employed for electrochemical deposition of metal nanostructures because of its chemical inertness, impermeability to gases and liquids, and high-temperature resistance.[14] Pre-modification of the GCE electrodes or additives in the electrolytes is necessary in certain cases for preparing metal nanostructures through electrochemical deposition.[15] To prevent the effects of additives or surfactants in electrochemical and analytical applications, a simple one-pot electrodeposition technique for the fabrication of metal nanostructured surfaces is receiving much attention.[16]

Palladium (Pd) has attracted much interest in the area of heterogeneous catalysis because of its high catalytic activity. Several studies have assessed the formation of Pd nanostructures on different substrates using electrodeposition. Flower-shaped Pd nanoparticles were synthesized by electrodeposition on an indium tin oxide (ITO) electrode with a thin polymer layer.[17] Pd nanodendrites were developed on the GCE surface by electrodeposition using ethylenediamine as an additive.[18] Recently, electrodeposition with no additives was applied to prepare different Pd nanostructures. Pd nanoflake[1] and triangular Pd Rod nanostructures[7] on the Au substrate, Pd nanodendrites[19] and nanourchins[20] on the ITO surface, and Pd nanothorns[21,22] on the carbon surface have been reported. Such Pd nanostructures showed good electrocatalytic performance. For the improvement of electrochemical efficiency, the preparation of various morphological Pd nanostructures is necessary.

To address environmental issues, researchers have particularly focused on clean energy sources such as electrochemical energy storage and conversion devices.[23–28]

Fuel cells are promising candidates for use as zero-emission energy conversion devices.[29–32] Although hydrogen fuel cells, alcohol-based fuel cells, and hydrazine fuel cells have been developed, their accessibility for commercial use remains uncertain because of safety, environmental, and storage issues.[33–36] To overcome these obstacles, ascorbic acid (AA) can be an alternative source of fuel in direct liquid fuel cells (DLFC). AA is a natural fuel source that produces nontoxic by-products during its oxidation, releases two electrons, and forms dehydroascorbic acid (DHA), as shown in Scheme 1.[37–41] The performance of the AA-based DLFC is dependent on the catalytic performance of AA electro-oxidation. The Pd metal is a promising catalyst for the enhancement of electro-oxidation of AA. Recent studies have shown that a Pd-based anode catalyst shows good catalytic performance for AA electro-oxidation.[42–44] In the alkaline condition, the Pd catalyst exhibits higher AA electro-oxidation than the acidic condition.[45] The different Pd morphological effect on the catalytic activity of AA electro-oxidation in alkaline conditions needs to be investigated.

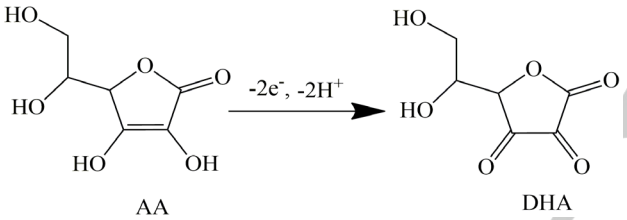

Scheme 1. Oxidation of AA.

In this work, we report unique Pd nanostructures electrodeposited on the GCE by constant potential mode using no additive or substrate surface pre-modification. The Pd nanostructures were defined as Christmas-tree-shaped Pd nanostructures. The fabrication process of these unique nanostructures was optimized. To our knowledge, this report is the first to demonstrate the formation of Christmas-tree-shaped Pd nanostructures on the GCE surface by electrodeposition. The catalytic activity of AA electro-oxidation was checked using the Christmas-tree-shaped Pd nanostructures on the GCE in the alkaline condition. The morphological effects and the mass activities of Pd on the catalytic activity of AA electro-oxidation in the alkaline condition were also studied.

Results and Discussion

Morphological and elemental analyses

We prepared five electrodes using constant potential mode (see experimental section) and designated them as Pd/GCE-0.1V_175S, Pd/GCE-0.1V_400S, Pd/GCE-0.1V_600S, Pd/GCE-0.4V_175S, and Pd/GCE-0.4V_400S, respectively, for the deposition conditions of -0.1 V for 175 s, -0.1 V for 400 s, -0.1 V for 600 s, -0.4 V for 175 s, and -0.4 V for 400 s. FE-SEM images of Pd/GCE-0.1V_400S are displayed in Figure 1(a-d). FE-SEM reveals the formation of Christmas-tree-shaped nanostructures. These nanostructures are distributed homogeneously on the GCE surface shown in Figure 1a. The high magnification images (Figure 1(b-d)) revealed the excellent form of the Christmas-tree-shaped nanostructures of 200–300 nm in size. These Pd nanostructures, confirmed by EDX, are unique and markedly different from previously-reported results such as nanoparticles, rod-like or dendritic structures.[7,19] The Christmas-tree-shaped Pd nanostructures on the GCE surface were electrodeposited using 15 mM Na_2PdCl_4 solution at a constant applied potential of −0.1 V for 400 s. We applied different potential and times to investigate the morphology of other modified electrodes, as shown in Supporting Information (Figure S1). Although we applied a potential of -0.1 V for 175 s (Figure S1a), the Christmas-tree-shaped Pd nanostructures did not form. The Pd/GCE-0.1V_600S has similar but not the same as Christmas-tree-shaped nanostructures (Figure S1b). The number of sharp edges of the nanostructures is less than the nanostructures deposited on the GCE for 400 s at -0.1 V (Figure 1d). The amount of metal deposition increased with deposition time. This increase engenders the formation of nanostructures having fewer sharp edges. The optimal electro-deposition time of 400 s provides the adequate formation of the Christmas-tree-shaped nanostructures with many sharp edges on the GCE at -0.1 V. Therefore, deposition time is an important parameter for unique nanostructure formation. To check the effect of applied potential, we applied a different potential -0.4 V for 175 and 400 s. FE-SEM images (Figure S1(c-d)) revealed that Pd was deposited randomly on the GCE surface and no Christmas-tree-shaped nanostructures were obtained. The precursor (Na_2PdCl_4) concentration controlled the morphology of the Pd deposits (Figure S2). Although applying deposition potential -0.1V for 400 s, lower Na_2PdCl_4 concentration (5 mM) resulted in Pd deposits with less-defined structures. Higher Na_2PdCl_4 concentration (30 mM) resulted in random Pd formations. So 15 mM Na_2PdCl_4 concentration is essential for the formation of Christmas-tree-shaped Pd nanostructures. The supporting electrolyte also performs a significant role in the development of vertically expanding Pd nanostructures. It is well known that specific sulfuric acid anion adsorption, such as SO_4^{2-} on Pd surfaces, can play a key role during electrodeposition in the vertical growth of Pd.[19] The diffusion-limited current at -0.1 V[7] and the deposition time of

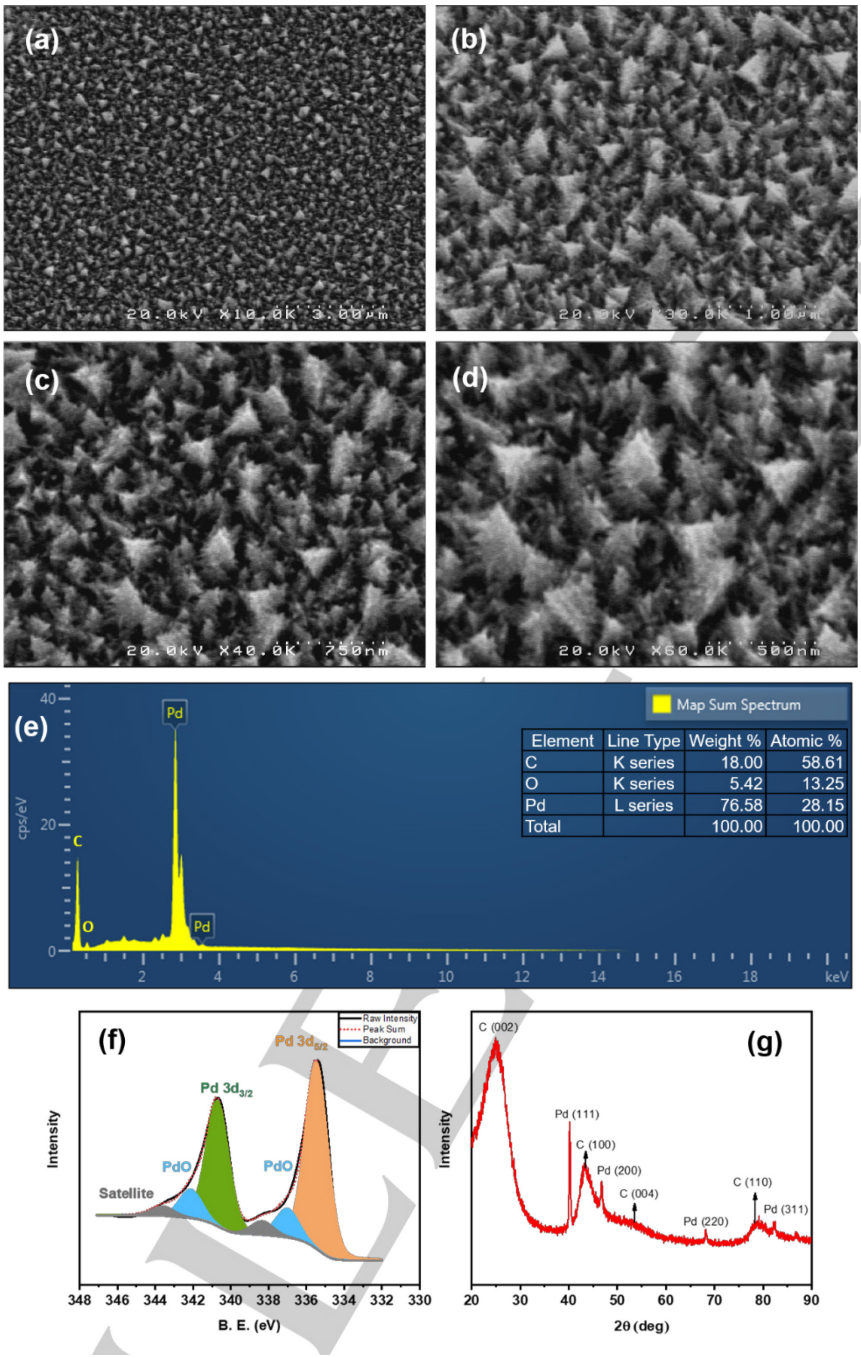

Figure 1. Characterizations of Pd/GCE-0.1V_400S: (a) low magnification FE-SEM image; (b), (c), and (d) high magnification FE-SEM image; (e) atomic ratio of elements by EDX analysis; (f) Pd 3d XPS spectrum; and (g) XRD pattern.

400 s as well as the concentration of precursor and supporting electrolyte anion SO_4^{2-} assist the formation of the Christmas-tree-shaped Pd nanostructures on the GCE.

Figure 1e shows the atomic ratio of the Pd/GCE-0.1V_400S. The C, O, and Pd elements are present in the Pd/GCE-0.1V_400S. The amount of Pd is quite high compared to other elements. So the Pd is successfully deposited on the GCE by the constant potential mode of electrodeposition. In the EDX analysis, the C element comes from the presence of GCE and a small amount of O element may attribute to the presence of PdO, which has been confirmed by XPS analysis. The XPS analysis was conducted for further confirmation of the oxidation state of the Pd in the Pd/GCE-0.1V_400S. The Pd 3d XPS spectrum showed two major peaks (Figure 1f). Those two peaks were separated by 5.2 eV having binding energies of 340.7 eV and 335.5 eV, respectively representing Pd ($3d_{3/2}$) and Pd ($3d_{5/2}$).[46–49] The XPS data revealed that the deposited Pd was in both metallic and oxide states in the Pd/GCE-0.1V_400S. The amount of PdO, found at

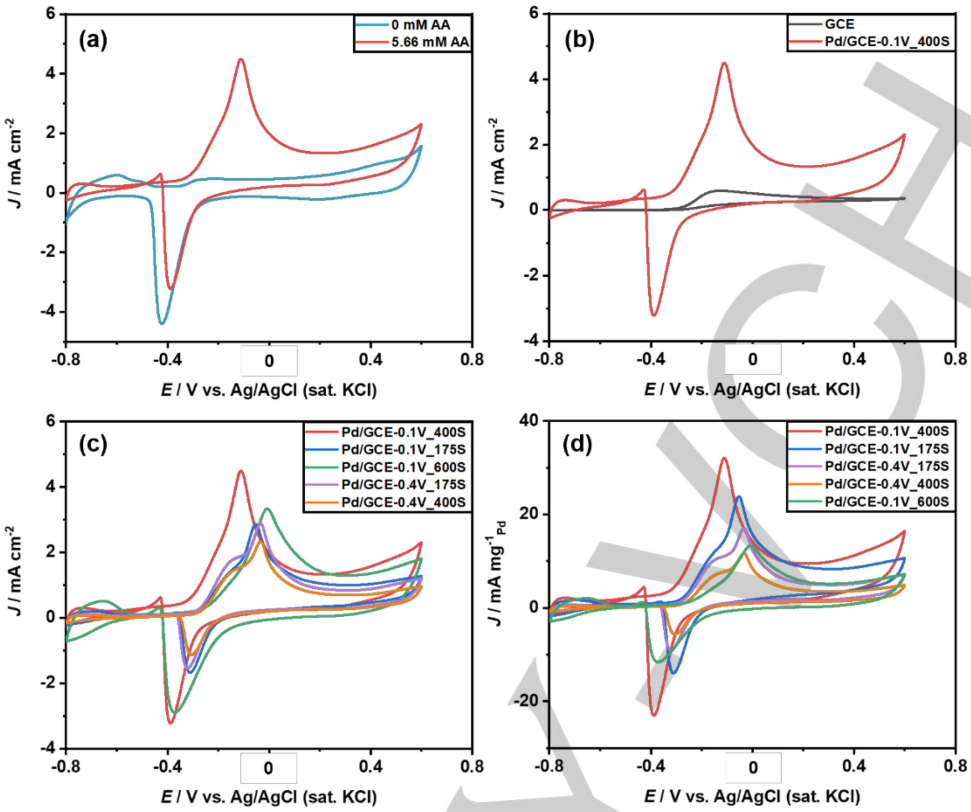

Figure 2. (a) Cyclic voltammograms of Pd/GCE-0.1V_400S in the absence (cyan line) and presence of 5.6 mM AA (red line) in 1 M KOH solution. (b) Catalytic activity comparison of bare GCE (black line), and Pd/GCE-0.1V_400S (red line) for 5.6 mM AA in 1 M KOH solution. (c) Response of AA electro-oxidation in 1 M KOH solution at Pd/GCE-0.1V_400S (red line), Pd/GCE-0.1V_175S (blue line), Pd/GCE-0.1V_600S (green line), Pd/GCE-0.4V_175S (violet line), and Pd/GCE-0.4V_400S (orange line). (d) Mass activities of Pd/GCE-0.1V_400S (red line), Pd/GCE-0.1V_175S (blue line), Pd/GCE-0.1V_600S (green line), Pd/GCE-0.4V_175S (violet line), and Pd/GCE-0.4V_400S (orange line). All the cyclic voltammograms above were taken with a 50 mV s^{-1} scan rate.

higher binding energy, was about 15% compared to the metallic Pd. Two satellite peaks were apparent at 343.6 eV and 338.3 eV.[50] These two satellite peaks are attributable to the high amount of Pd metallic state present in Pd/GCE-0.1V_400S. For the other modified electrodes, the Pd 3d XPS spectra showed similar features to those found for Pd/GCE-0.1V_400S (Figure S3). The Pd deposited on the GCE shows both metallic and oxide states. So different deposition conditions do not affect the oxidation state of the Pd deposit.

Figure 1g shows the XRD pattern obtained for Pd/GCE-0.1V_400S. The broad diffraction peak at 25.1° corresponds to the C (002) plane of graphite. The diffraction peaks at 43.3°, 54.5°, and 78.8° respectively correspond to the C (100), C (004), and C (110) planes.[14,51,52] These peaks appeared because of the presence of GCE. The diffraction peak at 40.2° corresponds to the Pd (111) plane.[53] Other diffraction peaks of Pd were found at 46.7°, 68.1°, and 82.3°, respectively corresponding to the Pd (200), Pd (220), and Pd (311) planes.[54] The XRD patterns of other modified electrodes are shown in Figure S4. The Pd (111) plane with a similar 2θ value corresponding to the Pd/GCE-0.1V_400S was found among those electrodes.

Electrocatalytic activity

The electrocatalytic performance of the Pd/GCE-0.1V_400S for AA electro-oxidation in alkaline conditions was investigated under different experimental conditions. The Christmas-tree-shaped Pd nanostructures on the GCE (Pd/GCE-0.1V_400S) were used to in Figure 2a. Cyclic voltammograms were recorded between -0.8 V and +0.7 V at a scan rate of 50 mV s^{-1} in the presence and absence of AA (5.6 mM) in 1 M KOH solution. The Pd/GCE-0.1V_400S (red line) shows an oxidation wave of AA at -0.1 V. An absence of AA in the 1 M KOH solution gives no oxidation peak (cyan line). A strong reduction peak at -0.4 V is attributed to the reduction of PdO to Pd.[55] We have also found a small oxidation peak around -0.2 V for the Pd/GCE-0.1V_400S in 1 M KOH

having no AA (see Figure 2a cyan line). This oxidation peak is due to the development of Pd^{2+} from Pd^0 in alkaline conditions.[56,57] Pd is first oxidized to form Pd^{2+} in an alkaline environment, which further improved the oxidation of AA. To elucidate the catalytic effects of the GCE and the Christmas-tree-shaped Pd nanostructures on the AA electro-oxidation, we performed the CV measurements. In Figure 2b, the voltammogram of the bare GCE (black line) shows a small AA oxidation peak compared with that of the Pd/GCE-0.1V_400S (red line). The Pd/GCE-0.1V_400S provides much higher current density (4.5 mA cm^{-2}) for AA electro-oxidation than the bare GCE (0.6 mA cm^{-2}) in 1 M KOH solution. The Pd plays a crucially important role in the excellent catalytic activity of the AA electro-oxidation in the alkaline condition.

We further evaluated the catalytic performance by comparing all the modified electrodes to investigate the influence of the unique nanostructures of the Pd for AA electro-oxidation. Figure 2c displays the response of all modified electrodes in the presence of 5.6 mM AA in KOH at a 50 mV s^{-1} scan rate. Among all electrodes, the Christmas-tree-shaped structure of the Pd/GCE-0.1V_400S showed the highest catalytic activity of AA electro-oxidation in 1 M KOH solution. The catalytic activity can be enhanced by increasing the electrode surface area. The electrochemical surface area (ESA) of all the electrodes was obtained by application of CV at different scan rates in 3.0 mM $K_3Fe(CN)_6$ solution (Figure S5) and was calculated using Randles–Sevcik equation as[58]

$$I_p = (2.69 \times 10^5) n^{3/2} A C D^{1/2} \upsilon^{1/2} \quad (1)$$

where I_p represents the peak current (A), n stands for the number of electron transfer during the redox process of $K_3Fe(CN)_6$, A represents the electrode area (cm^2), C denotes the concentration of the $K_3Fe(CN)_6$ solution (mol cm^{-3}), D is the diffusion coefficient of the $K_3Fe(CN)_6$ in units of cm^2 s^{-1}, and υ expresses the scan rate (V s^{-1}). The ESA of the Pd/GCE-0.1V_400S was 0.07 cm^{-2}, which is higher than Pd/GCE-0.1V_175S (0.05 cm^{-2}) and Pd/GCE-0.4V_175S (0.05 cm^{-2}). The ESA of Pd/GCE-0.4V_400S (0.07 cm^{-2}) is similar to that of Pd/GCE-0.1V_400S. Although these two electrodes have similar ESA, the morphological differences might have a strong effect on catalytic activities. From Figure 1d, the Christmas-tree-shaped nanostructures (Pd/GCE-0.1V_400S) have many sharp edges that can enhance the AA electro-oxidation. As a result, the current density increased. However, the ESA of the Pd/GCE-0.1V_600S (0.09 cm^{-2}) is higher than that of the Pd/GCE-0.1V_400S, but the catalytic activity is lower. The FE-SEM of the Pd/GCE-0.1V_600S (Figure S1b) showed fewer sharp edges of Christmas-tree-shaped

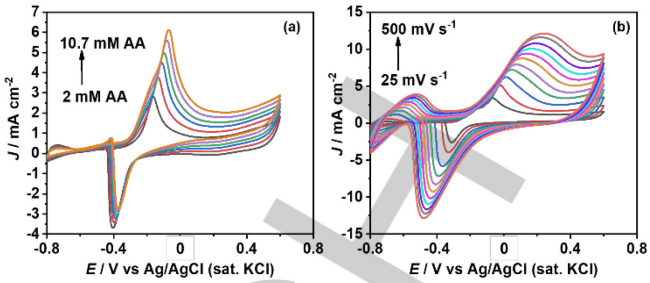

Figure 3. Cyclic voltammograms of Pd/GCE-0.1V_400S: (a) concentration effect of AA in 1 M KOH at 50 mV s^{-1} scan rate and (b) scan rate effect of 7.4 mM AA in 1 M KOH.

nanostructures than Pd/GCE-0.1V_400S (Figure 1d). The sharp edges of the Christmas-tree-shaped nanostructures make Pd/GCE-0.1V_400S superior for catalytic performance compared to other modified electrodes that have no such features. The ESA of the bare GCE is 0.06 cm^2, even less than Pd/GCE-0.1V 400S. Therefore, as seen in Figure 2b, the current density of the Pd/GCE-0.1V 400S electrode is superior to the bare GCE. The onset potential of AA electro-oxidation at the Pd/GCE-0.1V_400S is lower than all the prepared electrodes (Figure 2c). The Pd/GCE-0.1V_600S has almost similar onset potential with other electrodes except Pd/GCE-0.1V_400S. This behavior can be also explained by the morphological effect. Although Pd/GCE-0.1V 600S has a similar morphology to Pd/GCE-0.1V 400S, a fewer number of sharp edges make less catalytic reactive for AA electro-oxidation.

The morphological effects of Pd nanostructures to the AA electro-oxidation in 1 M KOH solution were investigated further through the mass activity of the modified electrodes. The mass activity of each electrode was calculated by normalization of the Pd mass loading at the electrode. For each electrode, the deposition quantity of Pd (in mg) is determined by the mass difference before and after the electrodeposition of Pd on the GCE. The calculated amounts of the Pd deposition were 0.12, 0.14, 0.17, 0.20, and 0.25 mg, respectively, for Pd/GCE-0.1V_175S, Pd/GCE-0.1V_400S, Pd/GCE-0.4V_175S, Pd/GCE-0.4V_400S, and Pd/GCE-0.1V_600S. Figure 2d presents the mass activity of the Pd/GCE-0.1V_400S (red line), Pd/GCE-0.1V_175S (blue line), Pd/GCE-0.1V_600S (green line), Pd/GCE-0.4V_175S (violet line), and Pd/GCE-0.4V_400S (orange line) in 1 M KOH solution. The calculated mass activity of the Pd/GCE-0.1V_400S is 32.1 mA mg_{Pd}^{-1}, which is 1.34, 1.91, 2.41 and 2.76 times as large, respectively, as those of Pd/GCE-0.1V_175S (23.9 mA mg_{Pd}^{-1}), Pd/GCE-0.4V_175S (16.8 mA mg_{Pd}^{-1}), Pd/GCE-0.1V_600S (13.3 mA mg_{Pd}^{-1}), and Pd/GCE-0.4V_400S (11.6 mA mg_{Pd}^{-1}). This result further proved that the unique Christmas-tree-shaped Pd

nanostructures with many sharp edges have good catalytic activity towards AA electro-oxidation in 1 M KOH solution.

We have further investigated the electrocatalytic behaviors of the modified electrodes in terms of electrochemically active sites of the catalyst. Electrochemical active surface area (ECSA) is a significant parameter that describes the number of electrochemically active sites concerning metal catalyst mass.[56]

$$ECSA = Q/sl \quad (2)$$

Where, *Q* is the coulombic charge of the metal oxide reduction peak, *s* is the proportionality constant =0.405 mC cm^{-2}, and *l* is the metal loading (g m^{-2}). The ECSA of all the electrodes is summarized in Table 1. It can be seen from Table 1 that the Pd/GCE-0.1V_400S exhibits a maximum ECSA value than other catalysts. That means the Pd/GCE-0.1V_400S has the highest active reaction center for electrocatalysis. The lower ECSA value of Pd/GCE-0.1V_600S is due to the presence of fewer catalytic active sites. This further proves that the Christmas-tree-shaped Pd nanostructures with many sharp edges make Pd/GCE-0.1V 400S electrode superior for AA electro-oxidation.

Table 1. ECSA of all the modified electrodes.

Name of the electrode	Metal loading (g m^{-2})	ECSA (m^2 gm^{-1})
Pd/GCE-0.1V_175S	24.0	0.75
Pd/GCE-0.1V_400S	20.0	0.81
Pd/GCE-0.1V_600S	18.9	0.74
Pd/GCE-0.4V_175S	40.0	0.20
Pd/GCE-0.4V_400S	35.7	0.13

Figure 3a presents the concentration influence of AA (2.0–10.7 mM) at the Pd/GCE-0.1V_400S surface at a scan rate of 50 mV s^{-1}. The oxidation current density increased concomitantly with increased AA concentration. The peak potential of AA oxidation shifted positively with increased concentration, which can be denoted as a diffusion-controlled reaction [12]. This shift is attributable to a disturbance of the mass transport processes of the analyte. The current can be explainable by the mass transport of analyte from the bulk of the solution to the electrode surface. As the concentration of AA increases, the diffusion process is disrupted, and the electrochemical system applies more potential to the re-establishment of mass transport. Therefore, the peak potential shifted positively. Figure 3b presents the scan rate effect on the current potential behaviors of 7.4 mM AA electro-oxidation in 1 M KOH solution. The oxidation peak of the AA molecules

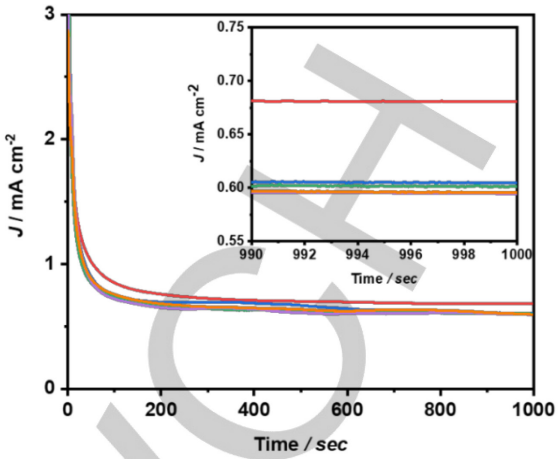

Figure 4. Chronoamperometry of 10.7 mM of AA at Pd/GCE-0.1V_400S (red line), Pd/GCE-0.1V_600S (green line), Pd/GCE-0.1V_175S (blue line), Pd/GCE-0.4V_175S (violet line), and Pd/GCE-0.4V_400S (orange line) in 1 M KOH solution (inset: magnification of chronoamperometric results for all electrodes from 990 to 1000 s).

increases concurrently with the increasing scan rate. Because of heterogeneous kinetics, the peak current increased with the scan rate. The plots of log peak current (I_p) differed linearly with the log (scan rate) is shown in Figure S6 with a slope value of 0.47. This observation suggests that the AA electro-oxidation follows a diffusion control process that has a theoretical 0.5 slope value.[14] This result also confirms that the AA electro-oxidation follows a diffusion-controlled reaction as described in the concentration-effect analysis. The peaks at -0.8 V to -0.7 V are increasing when the scan rate increased. This increase is attributable to the hydrogen adsorption and desorption behavior of the Pd catalyst.[55,56]

Stability of the modified electrodes

The stability check of the Pd/GCE-0.1V_400S (red line), Pd/GCE-0.1V_175S (blue line), Pd/GCE-0.1V_600S (green line), Pd/GCE-0.4V_175S (violet line), and Pd/GCE-0.4V_400S (orange line) for AA electro-oxidation in 1 M KOH by chronoamperometry, is shown in Figure 4. We applied the peak potential of the AA electro-oxidation for all modified electrodes for 1000 s. As shown in Figure 4, all curves that began with the dropping current density were attributable to the initial electro-oxidation of AA at the startup. Subsequently, the curves became flat and stable. The inset magnified figure in Figure 4 shows the current density from 990 to 1000 s for all electrodes. The Pd/GCE-0.1V_400S (red line)

showed good stability and excellent electrocatalytic activity compared with all other modified electrodes.

Table 2 summarizes information for recently reported AA electro-oxidation for comparison with our results. In all cases, the peak current density was determined by the peak current from the voltammetry measurement. The Pd/GCE-0.1V_400S shows the highest peak current density. The amperometry measurement is carried out for the measurement of lower detection limit (LOD) and the linear range value of the AA oxidation at Pd/GCE-0.1V_400S in 1 M KOH solution (Figure S7). With increasing concentration of the AA, the current response increased linearly. The LOD (1 μM) and the linear range value (1-950 μM) of AA electro-oxidation at Pd/GCE-0.1V_400S are comparable with the other catalyst mentioning in Table 2. This further confirms the excellent catalytic performance of the Pd/GCE-0.1V_400S catalyst for AA electro-oxidation.

Table 2. Comparison of the catalytic performance of AA electro-oxidation.

Electrode	Peak current density ($\mu A\ cm^{-2}$)	LOD (μM)	Linear range (μM)	Ref.
Pd/GCE-0.1V_400S	4500	1.0	1-950	This work
Pd/N-3D mesoporous C/GCE	2475	-	400-4000	[42]
CoPd/carbon/GCE	2465	0.1	0.1-3422	[43]
rMWCNTs/ Pd NTs/graphite	42	0.17	500-7500	[44]
Ag NPs/PVP/GCE	1650	0.47	2-150	[59]
CNO/$NiMoO_4$/ $MnWO_4$/GCE	-	0.33	1-100	[60]
PAP/ZrO_2NPs/CNTs /GCE	35	0.35	1-295	[61]

Note: rMWCNTs=reduced multi-walled carbon nanotubes; NTs=nanotubes; PVP= Polyvinylpyrrolidone; NPs= nanoparticles; CNO= carbon nanoonions; $NiMoO_4$= Nickel molybdate; $MnWO_4$= Manganese tungstate; PAP= Poly(aminopyrazine); ZrO_2NPs= Zirconium oxide nanoparticles; CNTs= carbon nanotubes (CNTs).

The selectivity of Pd/GCE-0.1V_400S for the AA oxidation was further evaluated by the amperometry measurements in 1 M KOH solution (Figure S8). Different interfering compounds such as KNO_3, $ZnSO_4$, $FeCl_2$, $MgCl_2$ were added to the AA-containing solution. Each of these interfering compounds has a very low current response, whereas AA has a distinguishable current response. This finding confirmed the high selectivity of the Pd/GCE-0.1V_400S electrode for AA oxidation. The analytical performance of the Pd/GCE-0.1V_400S was further investigated by the real sample analysis in 1 M KOH solution. We used the Vitamin C tablet and Vitamin C juice. The spiked samples had a recovery range ranging from 98.2% to 101.5% (Table S1), indicating the high efficiency of the Pd/GCE-0.1V_400S for AA oxidation.

The Christmas-tree-shaped Pd nanostructures on the GCE were optimized using constant potential and deposition time. The modified electrode exhibits excellent catalytic performance towards AA electro-oxidation with good stability in 1 M KOH. The Pd/GCE-0.1V_400S has a strong effect on the electrochemical performance due to many sharp edges. The excellent catalytic performance of our modified electrode has an immeasurable effect on the development of Pd-based catalysts for energy conversion devices and creates more interest in broad research audiences.

Conclusion

Unique Christmas-tree-shaped Pd nanostructures were developed on the GCE surface using one-step electrodeposition with a constant potential mode technique without additives and premodification of the electrode surfaces. The nanostructure morphology depended strongly on the deposition potential, time, precursor concentration, and supporting electrolyte during electrodeposition. We prepared different modified Pd/GCE electrodes by application of different deposition conditions, and the Christmas-tree-shaped Pd nanostructures with many sharp edges on the GCE (Pd/GCE-0.1V_400S) exhibited excellent catalytic performance for AA electro-oxidation in alkaline condition. Results also show that the Pd/GCE-0.1V_400S exhibits good electrochemical stability for AA electro-oxidation in 1 M KOH. The simple electrodeposition method used for the preparation of Christmas-tree-shaped Pd nanostructures on the GCE surface is expected to provide new opportunities for the future development of Pd-based energy conversion catalysts.

Supporting Information Summary

Supporting information includes chemicals and instruments, modification of GCE, characterization and measurements including FE-SEM images, XPS spectra, XRD patterns, Cyclic voltammograms, log (Ip) vs log (scan rate) plots, Amperometric measurement, interference effect of various compounds for AA electro-oxidation, real sample analysis by amperometric technique.

Acknowledgements

The authors would like to thank the Japan Advanced Institute of Science and Technology (JAIST) for an internal grant, which partially supported this research work. This work was partially supported by research funding from JSPS KAKENHI Grant Number JP21H00020.

Conflict of Interest

The authors declare no conflict of interest.

Keywords: Electrocatalysis • Electrochemistry • Electrodeposition • Palladium • Sharp edge nanostructures • Voltammetry

[1] H. Jeong, J. Kim, *ACS Appl. Mater. Interfaces* **2015**, *7*, 7129–7135.
[2] E. Katz, I. Willner, J. Wang, *Electroanalysis* **2004**, *16*, 19–44.
[3] M. J. Banholzer, J. E. Millstone, L. Qin, C. A. Mirkin, *Chem. Soc. Rev.* **2008**, *37*, 885.
[4] M. T. Islam, M. M. Hasan, M. F. Shabik, F. Islam, Y. Nagao, M. A. Hasnat, *Electrochim. Acta* **2020**, *360*, 136966.
[5] Y. Zhao, J. Qin, H. Xu, S. Gao, T. Jiang, S. Zhang, J. Jin, *Microchim. Acta* **2019**, *186*, 17.
[6] H. Kim, H. Park, D. K. Kim, S. Oh, I. Choi, S. K. Kim, *ACS Sustain. Chem. Eng.* **2019**, *7*, 8265–8273.
[7] S. Choi, H. Jeong, K. Choi, J. Y. Song, J. Kim, *ACS Appl. Mater. Interfaces* **2014**, *6*, 3002–3007.
[8] R. Ji, L. Wang, L. Yu, B. Geng, G. Wang, X. Zhang, *ACS Appl. Mater. Interfaces* **2013**, *5*, 10465–10472.
[9] L. Wang, L. Xu, H. Kuang, C. Xu, N. A. Kotov, *Acc. Chem. Res.* **2012**, *45*, 1916–1926.
[10] R. Shenhar, T. B. Norsten, V. M. Rotello, *Adv. Mater.* **2005**, *17*, 657–669.
[11] L. P. Bicelli, B. Bozzini, C. Mele, L. D'Urzo, *Int. J. Electrochem. Sci.* **2008**, *3*, 356–408.
[12] M. A. Hasnat, M. M. Hasan, N. Tanjila, M. M. Alam, M. M. Rahman, *Electrochim. Acta* **2017**, *225*, 105–113.
[13] Z. L. Zhou, T. F. Kang, Y. Zhang, S. Y. Cheng, *Microchim. Acta* **2009**, *164*, 133–138.
[14] M. M. Hasan, R. H. Rakib, M. A. Hasnat, Y. Nagao, *ACS Appl. Energy Mater.* **2020**, *3*, 2907–2915.
[15] M. M. Hossain, M. M. Islam, S. Ferdousi, T. Okajima, T. Ohsaka, *Electroanalysis* **2008**, *20*, 2435–2441.
[16] M. S. Alam, M. F. Shabik, M. M. Rahman, M. del Valle, M. A. Hasnat, *J. Electroanal. Chem.* **2019**, *839*, 1–8.
[17] Y. Li, G. Lu, X. Wu, G. Shi, *J. Phys. Chem. B* **2006**, *110*, 24585–24592.
[18] A. J. Wang, F. F. Li, Z. Bai, J. J. Feng, *Electrochim. Acta* **2012**, *85*, 685–692.
[19] Y. J. Song, J. Y. Kim, K. W. Park, *Cryst. Growth Des.* **2009**, *9*, 505–507.
[20] Y. Fang, S. Guo, C. Zhu, S. Dong, E. Wang, *Langmuir* **2010**, *26*, 17816–17820.
[21] H. Meng, F. Xie, J. Chen, P. K. Shen, *J. Mater. Chem.* **2011**, *21*, 11352.
[22] H. Meng, S. Sun, J. P. Masse, J. P. Dodelet, *Chem. Mater.* **2008**, *20*, 6998–7002.
[23] E. Mourad, L. Coustan, P. Lannelongue, D. Zigah, A. Mehdi, A. Vioux, S. A. Freunberger, F. Favier, O. Fontaine, *Nat. Mater.* **2017**, *16*, 446–453.
[24] N. Mahne, B. Schafzahl, C. Leypold, M. Leypold, S. Grumm, A. Leitgeb, G. A. Strohmeier, M. Wilkening, O. Fontaine, D. Kramer, C. Slugovc, S. M. Borisov, S. A. Freunberger, *Nat. Energy* **2017**, *2*, 1–9.
[25] Y. Nabil, S. Cavaliere, I. A. Harkness, J. D. B. Sharman, D. J. Jones, J. Rozière, *J. Power Sources* **2017**, *363*, 20–26.
[26] S. Nanda, R. Rana, Y. Zheng, J. A. Kozinski, A. K. Dalai, *Sustain. Energy Fuels* **2017**, *1*, 1232–1245.
[27] M. del Cueto, P. Ocón, J. M. L. Poyato, *J. Phys. Chem. C* **2015**, *119*, 2004–2009.
[28] S. Goodwin, D. A. Walsh, *ACS Appl. Mater. Interfaces* **2017**, *9*, 23654–23661.
[29] K. Dhara, R. M. Debiprosad, *Anal. Biochem.* **2019**, *586*, 113415.
[30] A. Mahajan, S. Banik, D. Majumdar, S. K. Bhattacharya, *ACS Omega* **2019**, *4*, 4658–4670.
[31] Z. Tao, Q. Zhang, X. Xi, G. Hou, L. Bi, *Electrochem. commun.* **2016**, *72*, 19–22.
[32] N. Fujiwara, S. Yamazaki, Z. Siroma, T. Ioroi, K. Yasuda, *Electrochem. commun.* **2006**, *8*, 720–724.
[33] D. Sebastián, A. Serov, I. Matanovic, K. Artyushkova, P. Atanassov, A. S. Aricò, V. Baglio, *Nano Energy* **2017**, *34*, 195–204.
[34] D. Sebastián, A. Serov, K. Artyushkova, J. Gordon, P. Atanassov, A. S. Aricò, V. Baglio, *ChemSusChem* **2016**, *9*, 1986–1995.
[35] D. K. Ross, *Vacuum* **2006**, *80*, 1084–1089.
[36] Z. M. Bhat, R. Thimmappa, M. C. Devendrachari, S. P. Shafi, S. Aralekallu, A. R. Kottaichamy, M. Gautam, M. O. Thotiyl, *J. Phys. Chem. Lett.* **2017**, *8*, 3523–3529.
[37] O. Muneeb, E. Do, T. Tran, D. Boyd, M. Huynh, G. Ghosn, J. L. Haan, *J. Power Sources* **2017**, *351*, 74–78.
[38] B. R. Sathe, *J. Electroanal. Chem.* **2017**, *799*, 609–616.
[39] M. Choun, H. J. Lee, J. Lee, *J. Energy Chem.* **2016**, *25*, 793–797.
[40] S. Uhm, J. Choi, S. T. Chung, J. Lee, *Electrochim. Acta* **2007**, *53*, 1731–1736.
[41] N. Fujiwara, S. Yamazaki, Z. Siroma, T. Ioroi, K. Yasuda, *J. Power Sources* **2007**, *167*, 32–38.
[42] A. Brouzgou, E. Gorbova, Y. Wang, S. Jing, A. Seretis, Z. Liang, P. Tsiakaras, *Ionics (Kiel).* **2019**, *25*, 6061–6070.
[43] F. Yang, J. Wang, Y. Cao, L. Zhang, X. Zhang, *Sensors Actuators B Chem.* **2014**, *205*, 20–25.
[44] C. D. Shruthi, Y. Venkataramanappa, G. S. Suresh, *J. Electrochem. Soc.* **2018**, *165*, B458–B465.
[45] O. Muneeb, E. Do, D. Boyd, J. Perez, J. L. Haan, *Appl. Energy* **2019**, *235*, 473–479.
[46] T. Sun, Z. Zhang, J. Xiao, C. Chen, F. Xiao, S. Wang, Y. Liu, *Sci. Rep.* **2013**, *3*, 2527.
[47] A. Bin Yousaf, M. Imran, A. Zeb, X. Xie, K. Liang, X. Zhou, C. Z. Yuan, A. W. Xu, *Catal. Sci. Technol.* **2016**, *6*, 4794–4801.
[48] Y. She, Z. Lu, W. Fan, S. Jewell, M. K. H. Leung, *J. Mater. Chem. A* **2014**, *2*, 3894.
[49] H. Ye, Y. Li, J. Chen, J. Sheng, X. Z. Fu, R. Sun, C. P. Wong, *J.*

Mater. Sci. **2018**, *53*, 15871–15881.

[50] G. Hu, F. Nitze, T. Sharifi, H. R. Barzegar, T. Wågberg, *J. Mater. Chem.* **2012**, *22*, 8541.

[51] Y. Wu, *Int. J. Electrochem. Sci.* **2017**, *12*, 1004–1013.

[52] A. A. Rafati, A. Afraz, A. Hajian, P. Assari, *Microchim. Acta* **2014**, *181*, 1999–2008.

[53] C. Lu, W. Guan, T. K. A. Hoang, Y. Li, T. N. L. Doan, H. Zhao, *Int. J. Electrochem. Sci.* **2015**, *10*, 5077–5085.

[54] Y. Lu, W. Chen, *ACS Catal.* **2012**, *2*, 84–90.

[55] X. L. Xing, Y. F. Zhao, H. Li, C. T. Wang, Q. X. Li, W. Bin Cai, *J. Electrochem. Soc.* **2018**, *165*, J3259–J3265.

[56] K. M. Hassan, A. A. Hathoot, R. Maher, M. Abdel Azzem, *RSC Adv.* **2018**, *8*, 15417–15426.

[57] B. Habibi, S. Mohammadyari, *Int. J. Hydrogen Energy* **2015**, *40*, 10833–10846.

[58] M. Abu Zahed, S. C. Barman, M. Sharifuzzaman, X. Xuan, J. S. Nah, J. Y. Park, *J. Electrochem. Soc.* **2018**, *165*, B840–B847.

[59] K. Karaboduk, *ChemistrySelect* **2019**, *4*, 6361–6369.

[60] M. Saleh Mohammadnia, E. Marzi Khosrowshahi, E. Naghian, A. Homayoun Keihan, E. Sohouli, M. E. Plonska-Brzezinska, Ali-Sobhani-Nasab, M. Rahimi-Nasrabadi, F. Ahmadi, *Microchem. J.* **2020**, *159*, 105470.

[61] S. Duzmen, A. K. Baytak, M. Aslanoglu, *Mater. Chem. Phys.* **2020**, *252*, 123170.

Entry for the Table of Contents

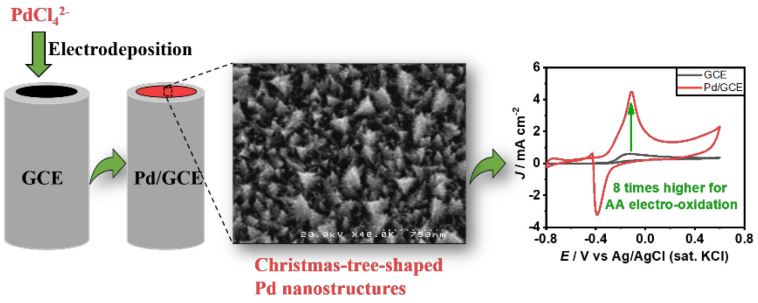

The unique Christmas-tree-shaped Pd nanostructures were generated through a simple electrodeposition technique on the glassy carbon electrode (GCE). The modified electrode showed excellent catalytic activity than the unmodified GCE for ascorbic acid electro-oxidation in alkaline condition. This high efficiency is derived from the many hierarchical edges of nanostructures.